

A design method for high fabrication tolerance integrated optical mode multiplexer

Bitao SHEN^{1,2}, Haowen SHU^{1,2}, Linjie ZHOU³ & Xingjun WANG^{1,2*}¹State Key Laboratory on Advanced Optical Communication Systems and Networks, Department of Electronics, School of Electronics Engineering and Computer Science, Peking University, Beijing 100871, China;²Nano-optoelectronics Frontier Center of Ministry of Education, Peking University, Beijing 100871, China;³State Key Laboratory of Advanced Optical Communication Systems and Networks, Department of Electronic Engineering, Shanghai Jiao Tong University, Shanghai 200240, China

Received 1 February 2020/Revised 18 April 2020/Accepted 23 April 2020/Published online 11 May 2020

Abstract The tapered asymmetric directional coupler has the potential to realize high fabrication tolerance and high transmission efficiency on-chip mode multiplexer. However, the geometry parameter selection of tapered structure remains empirical. In this paper, we propose a design method for the tapered structure based on genetic algorithm. Combined with the adjusted coupling equations and interpolation method, low-time-cost optimization can be realized. Three mode multiplexers (TE₀&TE₁, TE₀&TE₂ and TE₀&TE₅) are designed by our method. According to simulation results, the insertion loss of the designed devices is lower than 1.8 dB and the crosstalk is lower than -15 dB when the fabrication error is within required range (± 10 nm for TE₀&TE₂ and TE₀&TE₅, and ± 20 nm for TE₀&TE₁) in the bandwidth of 1.5–1.6 μm . In addition, the entire optimization process takes only 2 h for each device, which is around the time cost of a single 3D simulation.

Keywords mode multiplexer, directional coupler, taper structure, coupled-mode theory, genetic algorithm

Citation Shen B T, Shu H W, Zhou L J, et al. A design method for high fabrication tolerance integrated optical mode multiplexer. *Sci China Inf Sci*, 2020, 63(6): 160409, <https://doi.org/10.1007/s11432-020-2888-2>

1 Introduction

On-chip optical interconnection is a promising technical solution to overcome the bandwidth bottlenecks in inter-chip connection [1]. Different multiplexing technologies, such as wavelength division multiplexing [2], polarization division multiplexing [3,4] and mode division multiplexing [5,6], have been proposed to increase the capacity of single link for on-chip optical interconnection. Among them, mode division multiplexing provides a new dimension for the increase of link-capacity by utilizing various modes as channels [7,8]. Mode multiplexer, which is a critical component of mode division multiplexing system, has been widely studied. Various mode multiplexers have been designed based on multimode interferometers [9,10], Y-junctions [11,12], asymmetric directional couplers (ADC) [13,14] or ring resonators [15,16]. Among them, ADC has attracted much attention owing to its simple structure and design flow. However, this structure has a defect that it is sensitive to the width of waveguides which leads to relatively low fabrication error tolerance. As in [17], the fabrication error should be limited to 5 nm. Previous researches showed that the tapered structure, such as tapered [18], taper-etched [19] and non-planar tapered [20] structure can refine the fabrication tolerance characteristic. However, in those studies, the selection of optimal structural needed the traversal parameter analysis with 3D simulation, in which the time cost can be tremendous.

* Corresponding author (email: xjwang@pku.edu.cn)

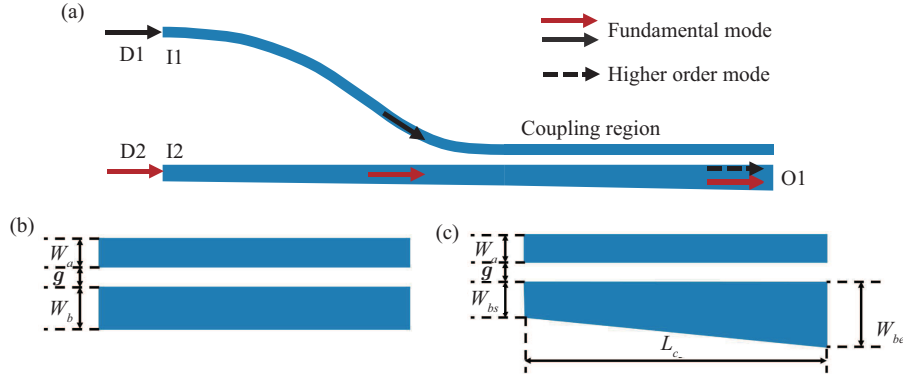


Figure 1 (Color online) (a) Schematic of the ADC based mode multiplexer; (b) detailed geometry parameters of the coupling region in a non-tapered ADC; (c) detailed geometry parameters of the coupling region in a tapered ADC.

In this paper, we propose a design method for tapered-ADC based high fabrication tolerance mode multiplexer, which focuses on how to select the geometry parameters of tapered structure proposed in [18]. With the combination of genetic algorithm and theoretical model based on the coupled mode theory (CMT), quick and accurate optimization of geometry parameters can be realized for required fabrication tolerance. To verify our method, a TE_0 & TE_1 , a TE_0 & TE_2 and a TE_0 & TE_5 mode multiplexer are designed with 20 nm, 10 nm and 10 nm fabrication tolerance respectively, whose insertion loss is lower than 1.8 dB in the bandwidth of 1.5–1.6 μm . Moreover, the time cost of the optimization process is close to that of a single 3D simulation, which means lower time cost compared with conventional methods.

2 Theoretical model

The ADC based mode multiplexer is a three-port device with two input ports (I1, I2) and one output port (O1), as shown in Figure 1(a). Two signal lights (D1, D2) will be input into the device through I1 and I2 respectively in fundamental mode. At the coupling region, D1 will be partly coupled into the bottom waveguide in higher order mode while the D2 will be confined in the bottom waveguide in fundamental mode. In this way, the signals carried in different modes can propagate through the same waveguide. The bottom waveguide can be seen as bus waveguide and the top one can be seen as assistance waveguide. Figure 1(b) shows the conventional non-tapered ADC and Figure 1(c) shows the tapered ADC used in this paper.

For the non-tapered ADC, the coupling process can be solved by CMT, while for the tapered ADC, the coupling process is usually solved by 3D simulation. Here, we derive the adjusted coupling equations based on previous CMT [21] to calculate the coupling process of tapered ADC.

According to CMT, the field of the whole tapered structure could be written as the sum of eigen-modes in different waveguides:

$$\begin{cases} \tilde{E} = A(z)\tilde{E}_1 + B(z)\tilde{E}_2, \\ \tilde{H} = A(z)\tilde{H}_1 + B(z)\tilde{H}_2, \end{cases} \quad (1)$$

where $A(z)$, $B(z)$ represent the amplitudes of the selected eigen-mode field in the assistance (bus) waveguide. \tilde{E}_p and \tilde{H}_p ($p = 1, 2$) are electric field intensity and magnetic field intensity of selected modes in relative waveguides. Unlike classical CMT, the two modes in the tapered structure are expressed as

$$\begin{cases} \tilde{E}_p = E_p(z) \exp[-j \int \beta_p(z) dz], \\ \tilde{H}_p = H_p(z) \exp[-j \int \beta_p(z) dz], \end{cases} \quad (2)$$

where β_p ($p = 1, 2$) represents propagation constant of the selected eigen mode. Similar to the derivation of coupled mode theory (Appendix A), by combining (1) with Maxwell's equations, we can get the

adjusted coupling equations for tapered structure:

$$\begin{cases} \frac{dA(z)}{dz} = -j\kappa_{12}(z)B(z) \exp \left[-j \int (\beta_2(z) - \beta_1(z)) dz \right], \\ \frac{dB(z)}{dz} = -j\kappa_{21}(z)A(z) \exp \left[+j \int (\beta_2(z) - \beta_1(z)) dz \right], \end{cases} \quad (3)$$

where κ_{pq} ($(p, q) = (1, 2), (2, 1)$) is the coupling index of the coupling system which can be calculated by

$$\kappa_{pq} = \frac{\omega \varepsilon_0 \iint_{S_p} \Delta \varepsilon \tilde{E}_p^* \cdot E_q dx dy}{\int_{-\infty}^{+\infty} \int_{-\infty}^{+\infty} u_z \cdot (\tilde{E}_p^* \times \tilde{H}_p + \tilde{E}_p \times \tilde{H}_p^*) dx dy}, \quad (4)$$

where ω is the circular frequency of the input light. ε_0 is the permittivity of vacuum and $\Delta \varepsilon$ is the difference of relative dielectric constants between the waveguide and the substrate. S_1 (S_2) is the region of assistance (bus) waveguide. The field distribution function and the propagation constant can be calculated by 2D simulation of a single waveguide.

Giving the structure and the initial amplitudes $A(0)$ and $B(0)$, $A(z)$ and $B(z)$ can be calculated using (3). This method avoids 3D simulation and only needs 2D simulation, which can decrease the time consumption greatly.

3 Design method

This section will introduce how to optimize the three key design parameters (W_{bs}, W_{be}, L_c) in a tapered ADC, taking TE₀&TE₁ multiplexer on SOI (silicon on insulator) for instance, to realize high coupling efficiency and required fabrication tolerance. Of all the parameters, the widths of waveguides have the greatest effect on performance [18, 22]. Thus, we only consider the effect of the width deviation ΔW .

For the tapered ADC based mode multiplexer, the design flow of the previous research includes three steps [18].

Step1. For a giving width of assistance waveguide, the width of bus waveguide is set to W_c as the original parameter, which makes the coupling system meet the phase matching condition.

Step2. Let the width of bus waveguide gradually change from $(W_c - \Delta W_c)$ to $(W_c + \Delta W_c)$.

Step3. Get the coupling region length L_c based on 3D simulation.

There are two main problems for the previous method. For one thing, owing to the large range of L_c , many times of 3D simulation should be calculated to get the proper value which leads to high time cost. For another thing, the selection of ΔW_c is not clear or it is hard to know whether the selected ΔW_c can meet the required tolerance. To solve these problems, in this paper, genetic algorithm [23] is employed to optimize the geometry parameters of tapered ADC for required fabrication tolerance.

3.1 The optimization variates

To simplify the optimization question, some parameters are set to common values. Here, we set the height of waveguides H to 220 nm, the gap between the two waveguides g to 200 nm, the width of assistance waveguide W_a to 400 nm and the wavelength λ to 1550 nm. Giving (W_{bs}, W_{be}, L_c) , the performance can be determined, where W_{bs} and W_{be} represent the starting and ending width of the tapered waveguide respectively and L_c represents the length of coupling region.

Therefore, (W_{bs}, W_{be}, L_c) are selected as optimization variates. Utilizing the genetic algorithm, the range of variates should be given as the scan range. As mentioned in previous research [18], the fabrication tolerance will be better if the $(W_{be} - W_{bs})$ is larger, at the expense of longer L_c . The range of L_c is determined based on requirement. The range of W_{bs} and W_{be} , or the range of the width of bus waveguide W_b , should ensure high coupling efficiency between selected modes and low coupling efficiency between undesired modes.

Figure 2(a) gives the relationship between effective refractive index and waveguide width for different modes. The coupling efficiency will be lower if the phase mismatching is larger. The phase mismatching δ is equal to $(\beta_2 - \beta_1)/2$. Thanks to large mode polarization dispersion of silicon-based rectangular

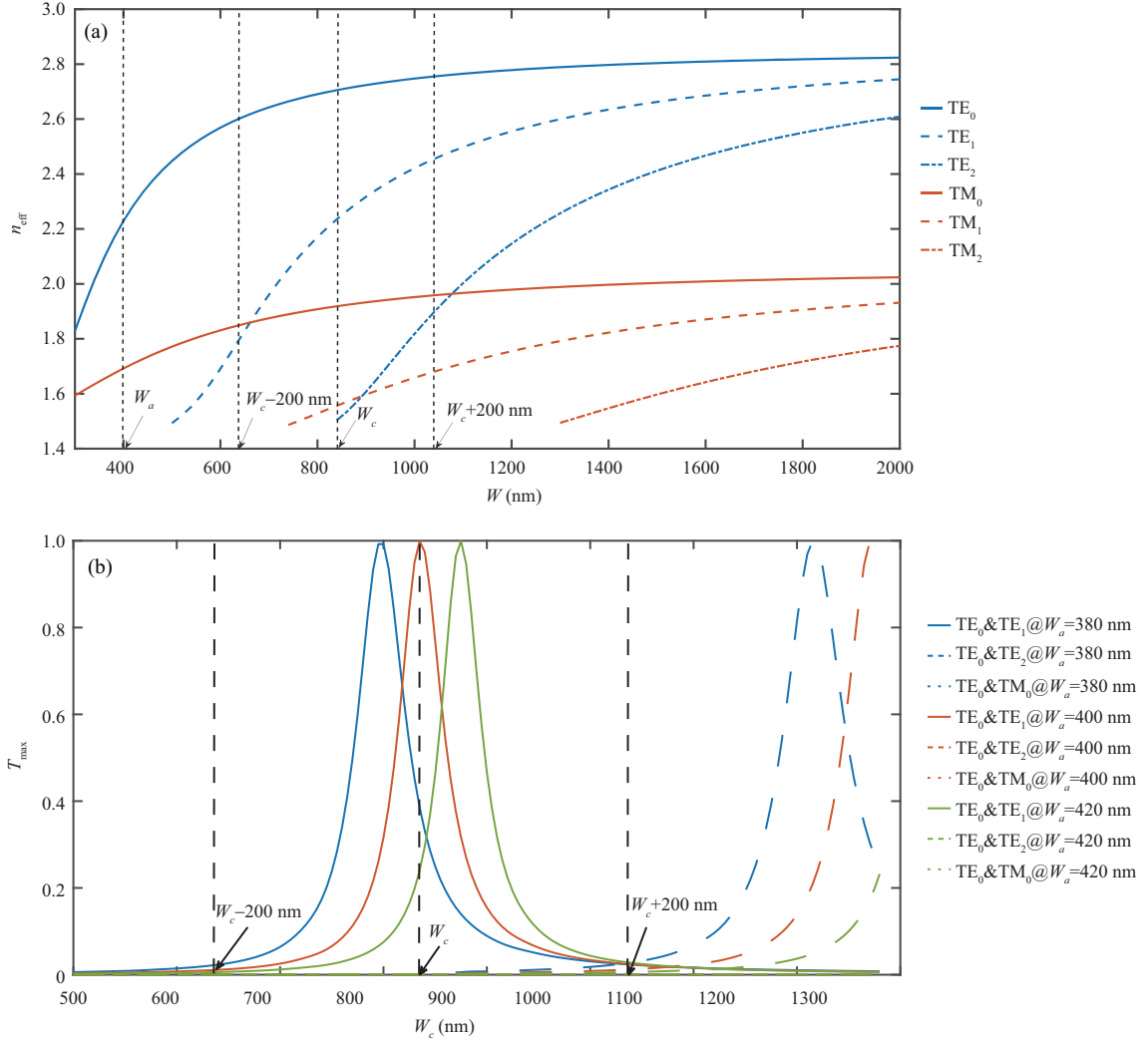


Figure 2 (Color online) (a) Relationship between effective refractive index and waveguide width for different modes; (b) relationship between the maximum transmission ratio and width of bus waveguide W_b for different W_a .

waveguide, the phase mismatching between the TE_0 in the bus waveguide and any modes in the assistance waveguide is large when W_b is around W_c , which means D2 will be almost completely confined in the bus waveguide in fundamental mode. Thus, we can consider the case where only D1 is input. The transmission ratio T is defined to quantify coupling efficiency,

$$T(W_a, W_{bs}, W_{be}, L_c) = \frac{P_{TE1}(L_c)}{P_{TE0}(0)}, \quad (5)$$

where $P_{TE1} = P_{TE1}(z)$ represents the power of TE_1 in the bus waveguide converted by TE_0 in the assistance waveguide, which is a function of the propagation distance z . $P_{TE0} = P_{TE0}(z)$ represents the power of TE_0 in the assistance waveguide. To determine the range of W_b , the relationship between the coupling efficiency and the width of bus waveguide for different modes and different W_a is given in Figure 2(b). The maximum transmission ratio T_{max} between TE_0 in the assistance waveguide and different modes in non-tapered bus waveguide is selected as characterization. T_{max} can be calculated based on CMT,

$$T_{\text{max}} = \frac{1}{1 + \left(\frac{\delta}{\kappa}\right)^2}. \quad (6)$$

According to Figure 2, we set the range of W_b to $(W_c - 200 \text{ nm}, W_c + 200 \text{ nm})$, where the transmission ratio remains higher enough for different W_a while the crosstalk is weak.

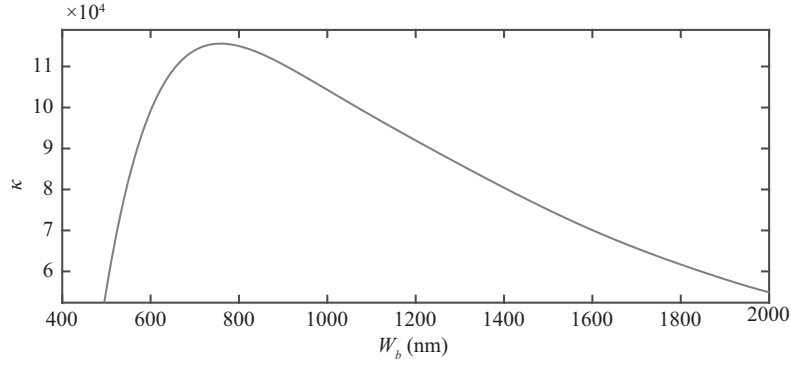


Figure 3 Relationship between the coupling index κ and the width of bus waveguide W_b when $W_a = 400$ nm.

3.2 The objective function

The transmission ratio T is defined to quantify coupling efficiency in Subsection 3.1. Taking the ΔW into account, the objective function is defined as

$$F(W_{bs}, W_{be}, L_c) = \prod_i T(W_a + \Delta W_i, W_{bs} + \Delta W_i, W_{be} + \Delta W_i, L_c), \quad (7)$$

where ΔW_i are several values that taken at equal intervals from the range of ΔW . For every parameter group generated by genetic algorithm, F can be calculated by using adjusted coupling equations. Giving W_a and (W_{bs}, W_{be}, L_c) , setting $A(0) = 1$ and $B(0) = 0$, the $B(L_c)$ can be calculated and

$$T(W_a, W_{bs}, W_{be}, L_c) = \frac{B^2(L_c)}{A^2(0)}. \quad (8)$$

κ and β can be given by using 2D simulation as motioned in Section 2. As shown in Figures 3 and 2(a), κ and β are functions of the waveguide width, where n_{eff} is the effective refractive index and equals to $\frac{\lambda\beta}{2\pi}$. We can calculate κ and β for different (W_a, W_b) before the optimization. Any κ and β values required during the calculation process can be obtained by interpolating. In this way, the number of 2D simulations required will be greatly reduced, which further decreases the time cost of the whole optimization process.

3.3 The genetic algorithm

According to the discussion above, the optimization problem can be expressed as

$$\begin{aligned} & \max F(W_{bs}, W_{be}, L_c) \\ \text{st. } & W_{bs} \in (W_c - 200 \text{ nm}, W_c + 200 \text{ nm}), \\ & W_{be} \in (W_c - 200 \text{ nm}, W_c + 200 \text{ nm}), \\ & L_c \in (0, L_{c\text{max}}). \end{aligned} \quad (9)$$

This problem can be solved by genetic algorithm. Figure 4 shows the flow chart of the genetic algorithm used in this paper, where Gen and GenMax represent the present and max number of generations. At the beginning, several groups of optimization variates (W_{bs}, W_{be}, L_c) will be generated and coded to binary values and the Gen will be set to 1. A group of (W_{bs}, W_{be}, L_c) is named as an individual and several individuals form a population. The value of F for every individual will be calculated as the fitness function. At the selecting process, individuals with higher F will tend to be copied to form a new population by the roulette wheel selection technique [23]. Individuals will form different pairs and a crossover operation will take place with probability $P_{\text{crossover}}$. If selected, the present pair of individuals will be changed by exchanging the randomly selected parts of the original chromosomes as shown in Figure 5(b). With probability $1 - P_{\text{crossover}}$, the pair will go directly to the mutation operator. At the

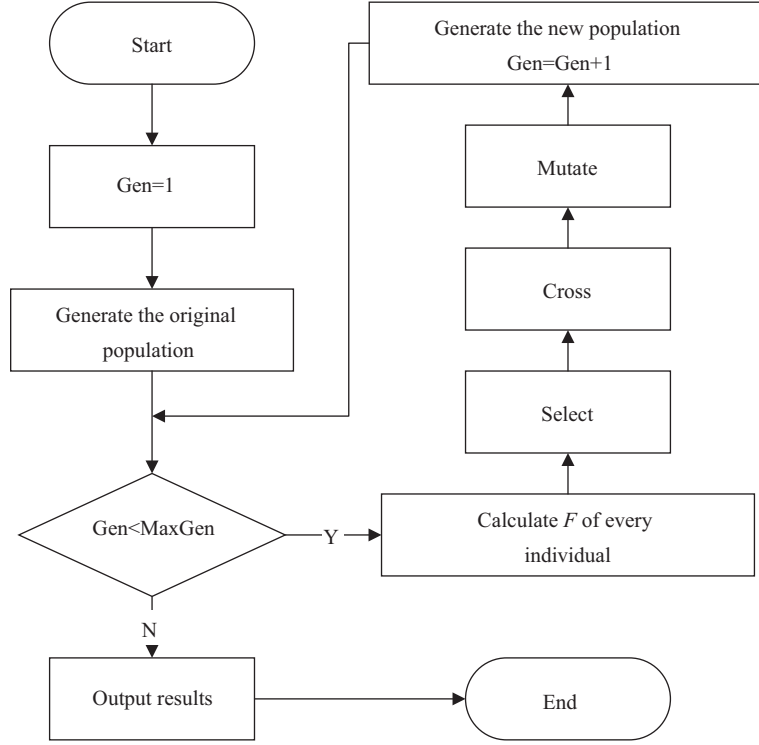


Figure 4 The flow chart of the typical genetic algorithm.

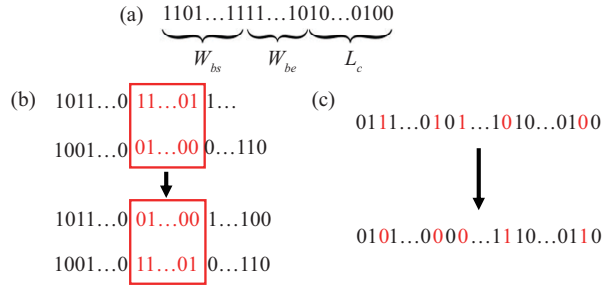


Figure 5 (Color online) Schematic diagram of (a) coding, (b) crossover and (c) mutation operations.

mutation section, for each gen of each individual, it will become the opposite with a low probability P_{mutation} as shown in Figure 5(c).

After selecting, crossing and mutating, the evolution of the old population is completed and the new one is generated. The evolution process will continue until $\text{Gen} > \text{MaxGen}$ and the parameter group with the maximum F is the required one.

Using the method above, an optimized tapered ADC structure can be obtained. If necessary, the optimized parameters can be fine-tuned based on 3D simulation.

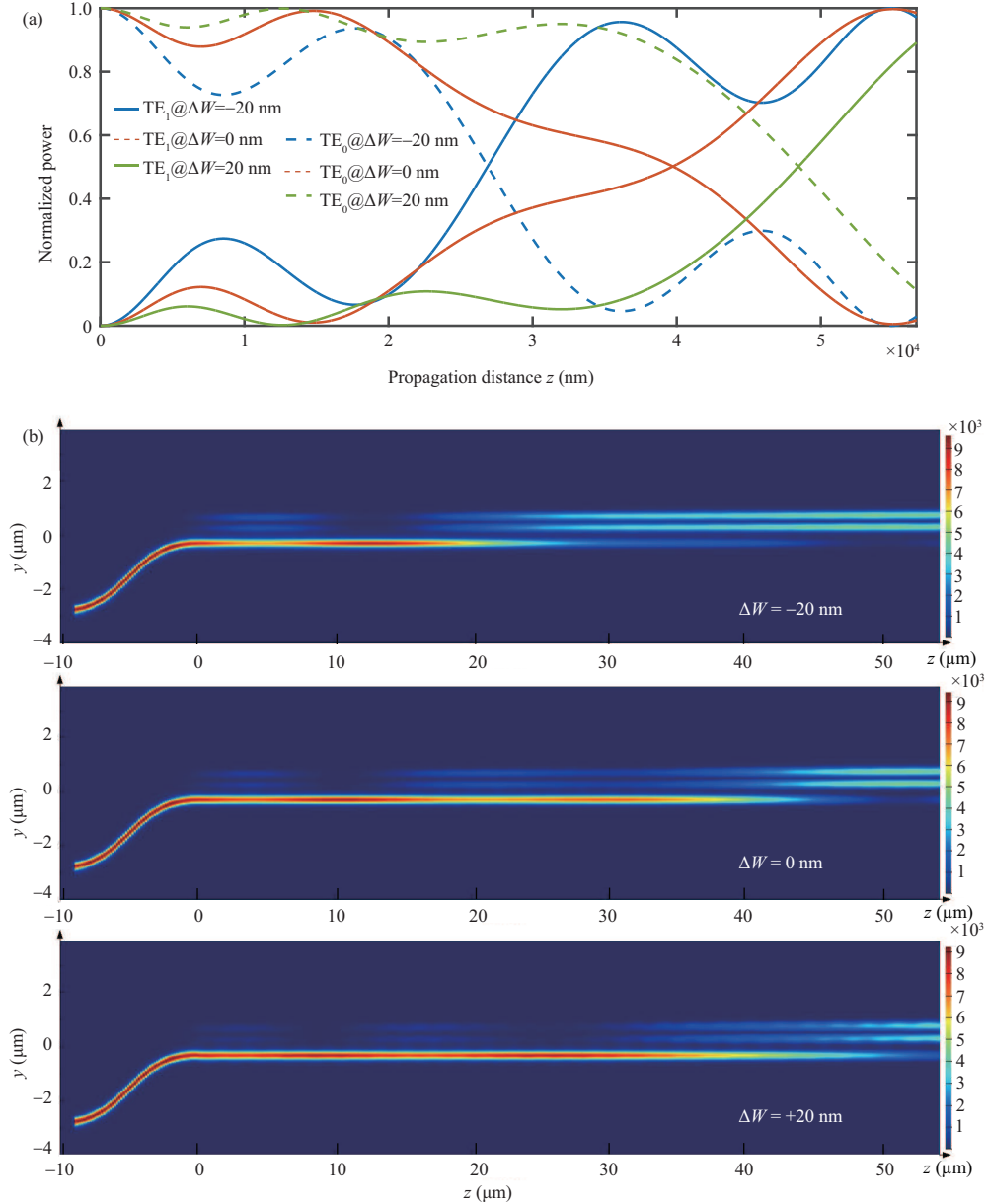
4 Results and discussion

Based on the method above, a $\text{TE}_0\&\text{TE}_1$ mode multiplexer with 20 nm fabrication tolerance, a $\text{TE}_0\&\text{TE}_2$ mode multiplexer with 10 nm fabrication tolerance and a $\text{TE}_0\&\text{TE}_5$ mode multiplexer with 10 nm fabrication tolerance on silicon-on-insulator (SOI) platform are designed. The W_a of the $\text{TE}_0\&\text{TE}_1$, the $\text{TE}_0\&\text{TE}_2$ and the $\text{TE}_0\&\text{TE}_5$ mode multiplexers are set to 400, 400 and 355 nm, respectively. The geometry parameters (W_{bs}, W_{be}, L_c) are shown in Table 1.

Figure 6 gives the coupling processes of the designed $\text{TE}_0\&\text{TE}_1$ mode multiplexer calculated by the

Table 1 The geometric parameters of designed devices

	W_{bs} (nm)	W_{be} (nm)	L_c (μm)
TE ₀ &TE ₁	761	879	54.08
TE ₀ &TE ₂	1222	1318	51.54
TE ₀ &TE ₅	2208	2428	58.23


Figure 6 (Color online) The coupling power variations along with the propagation length calculated by (a) the adjusted coupling equations and (b) 3D FDTD.

adjusted coupling equations mentioned in Section 2 and 3D FDTD (finite-difference time-domain method) for different ΔW . The normalized power of TE₁ in bus waveguides at the end of devices is 0.9531 (0.9659), 0.9073 (0.9462) and 0.8358 (0.8949), respectively for $\Delta W = -20$ nm, 0 nm and 20 nm calculated by 3D FDTD (adjusted coupling equation). The results calculated by our method are slightly different from that calculated by 3D FDTD. The deviation is partly owing to the coupling equation which is derived based on a series of assumptions. Besides, our method only considers the structure shown in Figure 1(c), while the coupling processes have occurred before reaching the ADC region. Despite the deviation, it can

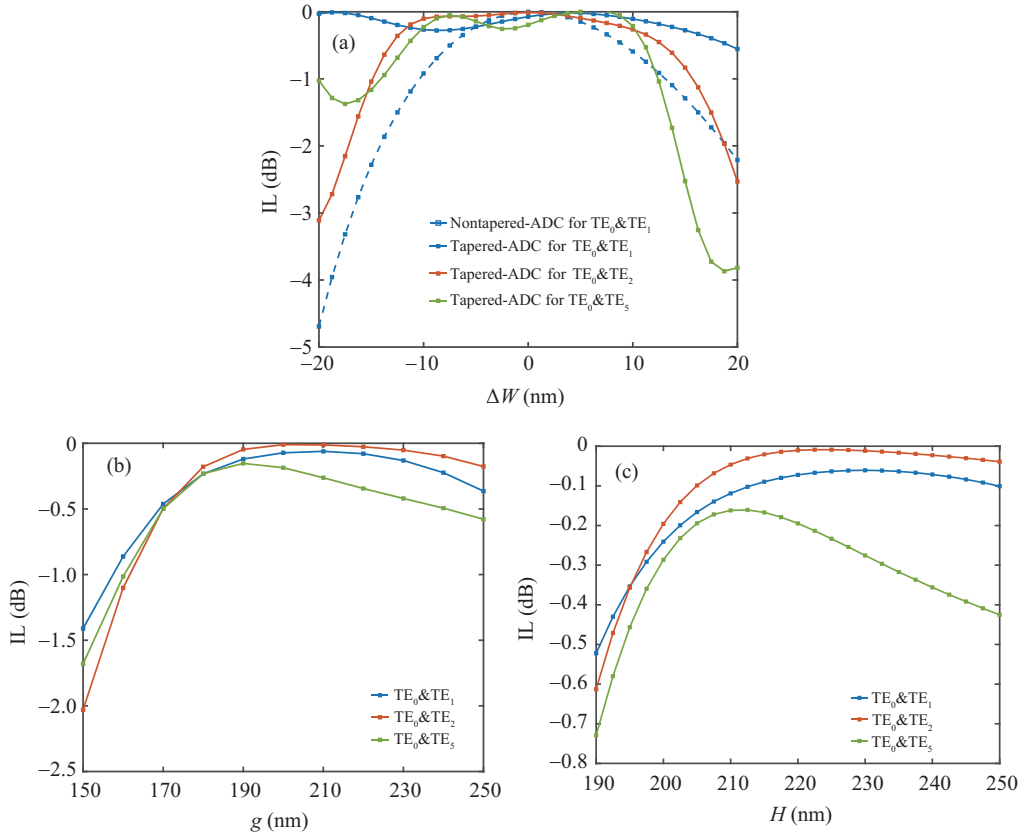


Figure 7 (Color online) (a) The comparison of insertion loss between a non-tapered ADC for TE_0 & TE_1 , whose (W_{bs}, W_{be}, L_c) is (836 nm, 836 nm, 20 μm), and the designed tapered ADCs when ΔW varies, at the wavelength of 1.55 μm , calculated by our methods. The insertion loss of designed devices as a function of the gap between (b) two waveguides g and (c) the height of waveguides H at the wavelength of 1.55 μm , calculated by our methods.

be seen that the coupling processes calculated by (3) is quite close to the one calculated by 3D FDTD.

As mentioned before, the calculation time cost of our method is lower than the traversal parameter analysis with 3D simulation. To get the optimal result, the coupling processes of 2000 (W_{bs}, W_{be}, L_c) groups are calculated and only 2 h are cost, which is around the time cost of a single 3D FDTD simulation. Figure 6 also shows that the coupling efficiency of the designed device remains high when the width of assistance waveguide varies.

To reveal the better fabrication tolerance characteristic of designed devices, an overall analysis for different geometric parameters is given in Figures 7 and 8, where the insertion loss IL is defined as

$$IL = 10 \log_{10}(T). \quad (10)$$

Figure 7(a) gives a comparison of the sensitivity to ΔW between the tapered structure and the non-tapered structure. By introducing the designed tapered structure, the sensitivity to the width deviation is eased. The insertion loss for different modes is exhibited in Figure 8. It can be seen that the crosstalk of the designed devices is mainly caused by TE_2 , TE_3 and TE_4 respectively while the crosstalk is lower than -15 dB for required fabrication error. Figure 8 also shows that the IL of the tapered ADCs we designed is lower than 1.8 dB, for ΔW varying in the required range and λ varying from 1.5 to 1.6 μm .

The impact of the other three parameters is shown in Figure 7(b) and (c). The devices are not sensitivity to the gap g and the height H . When the deviation of g and H is smaller than 30 nm, the insertion loss is lower than 1 dB.

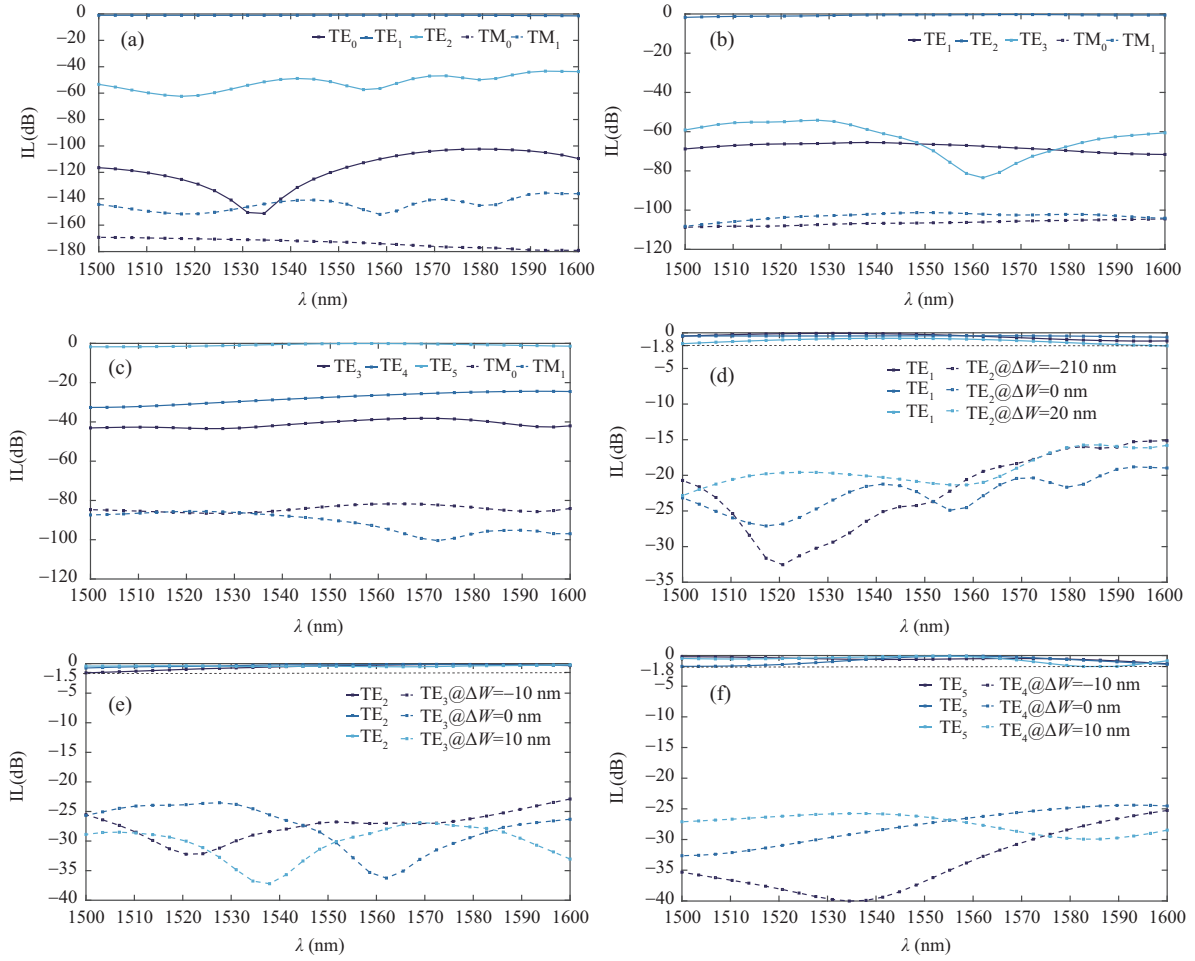


Figure 8 (Color online) The relationship between the insertion loss and wavelengths for different modes of (a) the TE₀&TE₁ mode multiplexer, (b) the TE₀&TE₂ mode multiplexer, (c) the TE₀&TE₅ mode multiplexer when $\Delta W = 0$, calculated by FDTD. The relationship between the insertion loss and wavelengths for different modes and different ΔW of (d) the TE₀&TE₁ mode multiplexer, (e) the TE₀&TE₂ mode multiplexer and (f) the TE₀&TE₅ mode multiplexer, calculated by FDTD.

5 Conclusion

In summary, we have proposed a design method for on-chip tapered-ADC based mode multiplexer which focuses on the selection of geometry parameters. Compared with previous methods, the adjusted coupling equations and genetic algorithm based method give a reasonable and accuracy selection method with low time cost. Simulation results show that the insertion loss of the designed mode multiplexers is lower than 1.8 dB for required fabrication error and the crosstalk to other modes is less than -15 dB. Moreover, the proposed method can serve as a general procedure for the design and optimization of any other tapered structure.

Acknowledgements This work was supported by National Natural Science Foundation of China (Grant Nos. 61635001, 61535002), Major International Cooperation and Exchange Program of the National Natural Science Foundation of China (Grant No. 61120106012), and Beijing Municipal Science & Technology Commission (Grant No. Z19110004819006).

References

- 1 Pavesi L, Lockwood D J. *Silicon Photonics III*. Berlin: Springer, 2016. 1–5
- 2 Fang Q, Liow T Y, Song J F, et al. WDM multi-channel silicon photonic receiver with 320 Gbps data transmission capability. *Opt Express*, 2010, 18: 5106–5113
- 3 Errando-Herranz C, Das S, Gylfason K B. Suspended polarization beam splitter on silicon-on-insulator. *Opt Express*, 2018, 26: 2675–2681

- 4 Yuan C, Dai J C, Jia H, et al. Design of a C-band polarization rotator-splitter based on a mode-evolution structure and an asymmetric directional coupler. *J Semiconduct*, 2018, 39: 105–111
- 5 Shi Y C, Chen J Y, Xu H N. Silicon-based on-chip diplexing/triplexing technologies and devices. *Sci China Inf Sci*, 2018, 61: 080402
- 6 Shu H, Shen B, Wang X, et al. A design guideline for mode (de)multiplexer based on integrated tapered asymmetric directional coupler. *IEEE Photon J*, 2019, 11: 1–12
- 7 Shu H, Deng Q, Wang X, et al. A polarization multiplexing optical circuit for efficient phase tuning. *IEEE Photon Technol Lett*, 2019, 31: 1549–1552
- 8 Li C L, Wu H, Tan Y, et al. Silicon-based on-chip hybrid (de)multiplexers. *Sci China Inf Sci*, 2018, 61: 080407
- 9 Han L, Liang S, Zhu H, et al. Two-mode de/multiplexer based on multimode interference couplers with a tilted joint as phase shifter. *Opt Lett*, 2015, 40: 518–521
- 10 Uematsu T, Ishizaka Y, Kawaguchi Y, et al. Design of a compact two-mode multi/demultiplexer consisting of multimode interference waveguides and a wavelength-insensitive phase shifter for mode-division multiplexing transmission. *J Lightw Technol*, 2012, 30: 2421–2426
- 11 Guo D, Chu T. Silicon mode (de)multiplexers with parameters optimized using shortcuts to adiabaticity. *Opt Express*, 2017, 25: 9160–9170
- 12 Chang W, Lu L, Ren X, et al. Ultra-compact mode (de)multiplexer based on subwavelength asymmetric Y-junction. *Opt Express*, 2018, 26: 8162–8170
- 13 Wang J, Chen P, Chen S, et al. Improved 8-channel silicon mode demultiplexer with grating polarizers. *Opt Express*, 2014, 22: 12799–12807
- 14 Liu L, Ding Y, Yvind K, et al. Efficient and compact TE-TM polarization converter built on silicon-on-insulator platform with a simple fabrication process. *Opt Lett*, 2011, 36: 1059–1061
- 15 Stern B, Zhu X, Chen C P, et al. On-chip mode-division multiplexing switch. *Optica*, 2015, 2: 530–535
- 16 Dorin B A, Ye W N. Two-mode division multiplexing in a silicon-on-insulator ring resonator. *Opt Express*, 2014, 22: 4547–4558
- 17 Pan C, Rahman B M A. Accurate analysis of the mode (de)multiplexer using asymmetric directional coupler. *J Lightw Technol*, 2016, 34: 2288–2296
- 18 Ding Y, Xu J, Da Ros F, et al. On-chip two-mode division multiplexing using tapered directional coupler-based mode multiplexer and demultiplexer. *Opt Express*, 2013, 21: 10376–10382
- 19 Sun Y, Xiong Y, Ye W N. Experimental demonstration of a two-mode (de)multiplexer based on a taper-etched directional coupler. *Opt Lett*, 2016, 41: 3743–3746
- 20 Zhao W K, Chen K X, Wu J Y. Broadband mode multiplexer formed with non-planar tapered directional couplers. *IEEE Photon Technol Lett*, 2019, 31: 169–172
- 21 Yariv A. Coupled-mode theory for guided-wave optics. *IEEE J Quantum Electron*, 1973, 9: 919–933
- 22 Mulugeta T, Rasras M. Silicon hybrid (de)multiplexer enabling simultaneous mode and wavelength-division multiplexing. *Opt Express*, 2015, 23: 943–949
- 23 Chambers L D. *The Practical Handbook of Genetic Algorithms: Applications*. 2nd ed. Boca Raton: CRC Press, 2000

Appendix A The derivation of the adjusted coupling equation

According to CMT, the field of the whole tapered structure could be written as the sum of egien-modes in different waveguides:

$$\begin{cases} \tilde{E} = A(z)\tilde{E}_1 + B(z)\tilde{E}_2, \\ \tilde{H} = A(z)\tilde{H}_1 + B(z)\tilde{H}_2. \end{cases} \quad (\text{A1})$$

Combining (A1) with Maxwell's equations, we can get

$$\begin{aligned} \frac{dA}{dz} + \frac{dB}{dz} \frac{\int_{-\infty}^{+\infty} \int_{-\infty}^{+\infty} u_z \cdot (\tilde{E}_1^* \times \tilde{H}_2 + \tilde{E}_2 \times \tilde{H}_1^*) dx dy}{\int_{-\infty}^{+\infty} \int_{-\infty}^{+\infty} u_z \cdot (\tilde{E}_1^* \times \tilde{H}_1 + \tilde{E}_1 \times \tilde{H}_1^*) dx dy} \\ + jA \frac{\omega \varepsilon_0 \int_{-\infty}^{+\infty} \int_{-\infty}^{+\infty} (N^2 - N_1^2) \tilde{E}_1^* \cdot \tilde{E}_1 dz dy}{\int_{-\infty}^{+\infty} \int_{-\infty}^{+\infty} u_z \cdot (\tilde{E}_1^* \times \tilde{H}_1 + \tilde{E}_1 \times \tilde{H}_1^*) dx dy} \\ + jA \frac{\omega \varepsilon_0 \int_{-\infty}^{+\infty} \int_{-\infty}^{+\infty} (N^2 - N_2^2) \tilde{E}_1^* \cdot \tilde{E}_2 dx dy}{\int_{-\infty}^{+\infty} \int_{-\infty}^{+\infty} u_z \cdot (\tilde{E}_1^* \times \tilde{H}_1 + \tilde{E}_1 \times \tilde{H}_1^*) dx dy} = 0, \end{aligned} \quad (\text{A2})$$

$$\begin{aligned} \frac{dB}{dz} + \frac{dA}{dz} \frac{\int_{-\infty}^{+\infty} \int_{-\infty}^{+\infty} u_z \cdot (\tilde{E}_2^* \times \tilde{H}_2 + \tilde{E}_2 \times \tilde{H}_1^*) dx dy}{\int_{-\infty}^{+\infty} \int_{-\infty}^{+\infty} u_z \cdot (\tilde{E}_1^* \times \tilde{H}_1 + \tilde{E}_1 \times \tilde{H}_1^*) dx dy} \\ + jA \frac{\omega \varepsilon_0 \int_{-\infty}^{+\infty} \int_{-\infty}^{+\infty} (N^2 - N_1^2) \tilde{E}_1^* \cdot \tilde{E}_1 dx dy}{\int_{-\infty}^{+\infty} \int_{-\infty}^{+\infty} u_z \cdot (\tilde{E}_1^* \times \tilde{H}_1 + \tilde{E}_1 \times \tilde{H}_1^*) dx dy} \\ + jA \frac{\omega \varepsilon_0 \int_{-\infty}^{+\infty} \int_{-\infty}^{+\infty} (N^2 - N_2^2) \tilde{E}_1^* \cdot \tilde{E}_2 dx dy}{\int_{-\infty}^{+\infty} \int_{-\infty}^{+\infty} u_z \cdot (\tilde{E}_1^* \times \tilde{H}_1 + \tilde{E}_1 \times \tilde{H}_1^*) dx dy} = 0. \end{aligned} \quad (\text{A3})$$

For a tapered ADC structure, the eigen modes in the two waveguide are given by

$$\begin{cases} \tilde{E}_p = E_p(z) \exp \left[-j \int \beta_p(z) dz \right], \\ \tilde{H}_p = H_p(z) \exp \left[-j \int \beta_p(z) dz \right]. \end{cases} \quad (\text{A4})$$

Substituting (A4) into (A2) and (A3), the coupling equations can be expressed as

$$\begin{aligned} \frac{dA}{dz} + c_{12}(z) \frac{dB}{dz} \exp \left[-j \int (\beta_2(z) - \beta_1(z)) dz \right] + j\chi_1(z)A \\ + j\kappa_{12}(z)B \exp \left[-j \int (\beta_2(z) - \beta_1(z)) dz \right] = 0, \end{aligned} \quad (\text{A5})$$

$$\begin{aligned} \frac{dB}{dz} + c_{21}(z) \frac{dA}{dz} \exp \left[+j \int (\beta_2(z) - \beta_1(z)) dz \right] + j\chi_2(z)B \\ + j\kappa_{21}(z)A \exp \left[+j \int (\beta_2(z) - \beta_1(z)) dz \right] = 0. \end{aligned} \quad (\text{A6})$$

Ignoring c_{pq} and χ_p , we can get the simplified coupling equations:

$$\begin{aligned} \frac{dA}{dz} &= -j\kappa_{12}(z)B \exp \left[-j \int (\beta_2(z) - \beta_1(z)) dz \right], \\ \frac{dB}{dz} &= -j\kappa_{21}(z)A \exp \left[+j \int (\beta_2(z) - \beta_1(z)) dz \right]. \end{aligned} \quad (\text{A7})$$